# Nanoscale

Accepted Manuscript


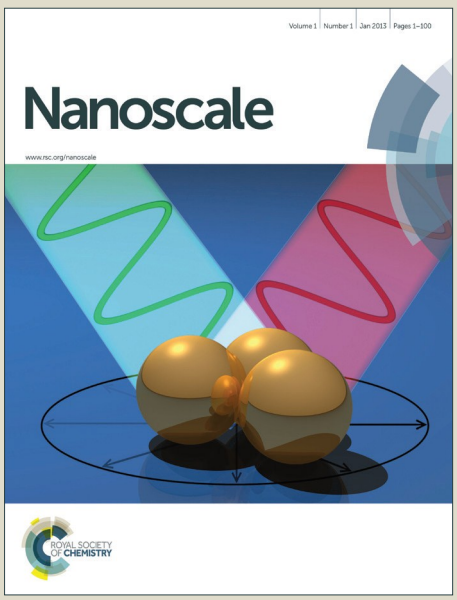





ROYAL SOCIETY OF CHEMISTRY

www.rsc.org/nanoscale

# Weathering of a Carbon Nanotube / Epoxy Nanocomposite under UV Light and in Water Bath: Impact on Abraded Particles

Lukas Schlagenhauf[a,b,c], Bahareh Kianfar[c], Tina Buerki-Thurnherr[d], , Yu-Ying Kuo[b,c], Adrian Wichser[b], Frank Nüesch[a], Peter Wick[d], and Jing Wang[b,c*].

[a]Laboratory for Functional Polymers, Empa - Swiss Federal Laboratories for Materials Science and Technology, Dübendorf, Switzerland;

[b]Laboratory for Advanced Analytical Technologies, Empa - Swiss Federal Laboratories for Materials Science and Technology, Dübendorf, Switzerland;

[c]Institute of Environmental Engineering, Swiss Federal Institute of Technology Zurich, Zurich, Switzerland;

[d]Laboratory for Particles-Biology Interactions, Empa - Swiss Federal Laboratories for Materials Science and Technology, St. Gallen, Switzerland.

**Corresponding author**: Jing Wang; Jing.Wang@ifu.baug.ethz.ch; Institute of Environmental Engineering, ETH Zürich, CH-8093 Zürich, Switzerland; Tel: +41 58 765 6115

## ABSTRACT

Weathering processes can influence the surface properties of composites with incorporated nanoparticles. These changes may affect the release behavior of nanoparticles when an abrasion process is applied. Therefore, the influence of two different weathering processes, immersion in water and exposure to UV light, on the properties of abraded particles from a carbon nanotube (CNT)/epoxy nanocomposite was investigated. The investigation included the measurement of the weathering impact on the surface chemistry of the exposed samples, the particle size of abraded particles, the quantity of exposed CNTs in the respirable part of the abraded particles, and the toxicity of abraded particles, measured by *in vitro* toxicity tests using the THP-1 monocyte-derived macrophages.

The results showed that weathering by immersion in water had no influence on the properties of abraded particles. The exposure to UV light caused a degradation of the epoxy on the surface, followed by delamination of an approx. 2.5 µm thick layer. An increased quantity of exposed CNTs in abraded particles was not found; on the contrary, longer exposure times decreased the released fraction of CNTs from 0.6 % to 0.4 %. The toxicity tests revealed that abraded particles from the nanocomposites did not induce additional acute cytotoxic effects compared to particles from the neat epoxy.


## 1. INTRODUCTION

Embedding carbon nanotubes (CNTs) in polymers can enhance the material performance. They influence the mechanical properties (e.g. higher modulus, higher fracture toughness, higher abrasion and wear resistance) [1–3], can reduce the permeability [4], or can lower the flammability [5,6]. Further, additional properties are added to the polymer such as the electrical and the thermal conductivity [7,8]. Nowadays, CNT nanocomposites are already used for several

applications in different industries, e.g. automotive, aerospace, defense, electronics, energy, and sporting goods [9].

Because of the high aspect ratio and biopersistent nature of CNTs, concerns have been raised that CNT composites can pose a risk to producers and consumers if the CNTs are released into the environment [10–13].The potential for a release of CNTs from nanocomposites, either by abrasion, weathering, or fire, has already been investigated in several studies [14]. When an abrasion process is applied, the release of CNTs mainly depends on the used material [15], the quantity of added CNTs [16], or on the distribution of the CNTs [17,18]. From weathering processes, i.e. immersion in water, exposure to UV light, or heat, no release of CNTs has been detected so far.

UV weathering experiments have shown that a degradation of the polymer surface can cause the release of silica nanoparticles from nanocomposites[19]. When CNTs were used as the filler material, a network of CNTs was generated on the surface. This network was relatively stable and the CNTs could only be released when strong shearing forces were applied [20]. Another weathering process is the uptake of water caused by high relative humidity (RH) or by immersion in liquids. The diffusion of water into the polymer matrix can cause permanent [21,22] or reversible [23] changes in the material properties. The release of CNTs from water weakened composites was not investigated yet, neither by leaching [9] nor by abrasion processes.

There are numerous *in vitro* and *in vivo* studies demonstrating that CNTs, particularly long multi-walled CNTs (MWCNTs), elicit various adverse effects ranging from frustrated phagocytosis to fibrosis and neo-plastic-like transformation [24–26]. Apparently, the toxicity depends strongly on the physicochemical properties of CNTs such as their length, rigidity and biopersistence. Considering the controversial discussion about the potential toxicity of CNTs, it is important to understand if abraded particles from CNT composites exhibit any of these potential adverse effects. In addition, weathering of CNT composites may lead to the release

of abraded particles with different properties as compared to non-aged nanocomposites, possibly inducing distinct cellular responses. The current knowledge on the toxicity of abraded particles from CNT composites is relatively sparse [18,27–32]. It appears that all toxic effects observed so far were predominantly from the matrix material, and abraded particles from CNT containing composites did not show any additional toxicity as compared to particles from neat matrix samples.

The absence of additional toxicity effect is related to the low concentration of exposed CNTs in the abraded particles. After weathering, the amount of released CNTs can be changed due to exposure of CNTs on the surface by UV light and/or weakening of the matrix. No results have been published on abrasion of weathered samples.

Here we report the first study on the impact of weathering on the properties of abraded particles from a MWCNT/epoxy nanocomposite, e.g. on the particle size, the release of free standing MWCNTs, the quantity of exposed MWCNTs, and the toxicity. For the investigated nanocomposite no release of free standing MWCNTs was detected when the untreated sample was abraded [18]. Two different weathering processes were mimicked, immersion in a water bath and exposure to UV light. For immersion in water, the kinetics of the water uptake was determined. The surface degradation of the samples was characterized by attenuated total reflectance Fourier transform infrared spectroscopy (ATR-FTIR) and by imaging of the topography. Further, the particle size distribution and the microstructure of abraded particles were investigated after usage of the Taber Abraser, a widely used device to simulate sanding processes with its own international standards (e.g., ISO 7784-2:1997 and ASTM G195-08). The quantity of exposed CNTs, i.e. protruding and free standing CNTs, in the respirable part (particulate matter below 1 μm or $PM_1$) of the abraded particles was determined and the toxicity of abraded particles, including the possible co-released CNTs and their catalysts, from weathered samples was measured with *in vitro* cell tests by mimicking a single-dose

inhalation scenario using the THP-1 monocyte-derived macrophages; both methods are described in another study [18].

## 2. MATERIALS & METHODS

### 2.1 SAMPLE PREPARATION

MWCNTs (Baytubes, C150p; length 1 – 10 µm) were supplied by Bayer Material Science AG (Characteristic properties of the Baytubes from the manufacturer [33] and our previous studies [18, 34, 35] are presented in Table S.1 in the supplemental information SI). The used epoxy resin was Araldite GY 250 (Huntsman, USA) based on bisphenol A. The curing agent was the polytheramine Jeffamine D-230 (Huntsman, USA) and the resin/hardener ratio was 100:32. For sample preparation, the MWCNTs were dispersed in the epoxy resin first for 30 min by ultrasonication and then by three-roll milling (SDY200, Bühler AG, Switzerland) at 30 °C and at a gap pressure of 1 MPa. The milling process was applied three times. After mixing with the curing agent, the composite was cured at 80 °C for 12 h, followed by post curing at 120 °C for 4 h. Characterization of the CNTs after dispersion in epoxy was performed in previous studies [1]. The CNT length distribution following the three-roll milling was found to be 0.7 ± 0.2 µm, indicating that the CNTs were chopped and shortened compared to the neat CNTs. Microscopic measurement confirmed good CNT dispersion in epoxy before curing. During the curing process some re-agglomeration occurred due to the higher mobility of CNTs at elevated temperatures.

Samples with various sizes were used in the experiments. For the investigation of the water uptake and the changes on the surface, samples were cut into pieces of 30 mm × 30 mm × 4 mm; the samples for weathering then abrasion experiments had a size of 100 mm × 85 mm × 4 mm. Three different kinds of samples were prepared, with 0 wt%, 0.1 wt%, or 1 wt% of MWCNTs. For the CNT-epoxy system, previous studies [1] showed the

mechanical properties were significantly improved when the added MWCNT concentration was < 1 wt%. Further increase of the MWCNT concentration only slightly improved the properties if at all. It was also observed that strong agglomeration occurred at >5% CNT content and concomitantly the mechanical properties degraded. Therefore we used the optimal concentration of around one percent. Such CNT filler concentrations are also common in commercial products (e.g. ZNT-boost, Zyvex [36]) and for research [19, 27, 37].

## 2.2 WEATHERING EXPERIMENTS

Prior to the water uptake experiment, the samples were cleaned by ethanol and dried under vacuum in a furnace at 40 °C for seven days. The samples were immersed in de-ionized water and the weight gain was determined by periodical weighing of the samples. Six samples per data point were measured and three different temperatures were investigated, 50 °C, 70 °C, and 90 °C. Samples for abrasion experiments were immersed in water at 70 °C for 1000 h.

The exposure to UV light was carried out in an accelerated weathering tester (QUV, Q-Lab Corporation, Cleveland, OH), equipped with a UVA-340 lamp (0.89 W/m$^2$ at 340 nm). This corresponds approx. to the light intensity in Florida at noon. The temperature was set to 60 °C and the RH was kept below 5 %. The samples were exposed to the UV light for five different durations, 200 h, 500 h, 750 h, 1000 h, and 1500 h.

## 2.3 CHARACTERIZATION OF WEATHERING IMPACTS

### 2.3.1 WATER UPTAKE

The relative weight increase of the water bath samples was calculated with Eq. 1,

$$M_t(\%) = \frac{W_t - W_0}{W_0} \cdot 100\% \quad (1)$$

where $M_t$ is the relative weight increase, $W_0$ the weight of the sample before immersion in the water bath, and $W_t$ the weight of the sample at immersion time $t$. To determine the diffusion constant, the water uptake curves were fitted according to Liu *et al.* [38, 39] with Fick's law (Eq. 2)

$$\frac{M_t}{M_\infty} = \left[1 - \sum_{n=0}^{\infty} \frac{8}{(2n+1)^2\pi^2} \cdot exp\left[\frac{-D_T(2n+1)^2\pi^2 t}{4l^2}\right]\right] \quad (2)$$

where $M_\infty$ is the maximum relative water uptake, $D_T$ the diffusion coefficient of the specific temperature, and $l$ is the sample thickness. The activation energy was obtained by fitting the diffusion coefficients of different temperatures with the Arrhenius equation (Eq. 3)

$$D = D_T \cdot exp\left(-\frac{E_a}{RT}\right) \quad (3)$$

where $D$ is the diffusion constant, $E_a$ the activation energy, $R$ the gas constant, and $T$ the temperature.

### 2.3.2 SURFACE TOPOGRAPHY AND CHEMISTRY

The topography of the samples was imaged by scanning electron microscopy (SEM) (Nova NanoSEM 230, FEI, Hillsboro, OR) and by atomic force microscopy (AFM) (Mobile S equipped with the large scan head, Nanosurf, Liestal, Switzerland). The impact on the weathering processes on the surface chemistry was investigated by ATR-FTIR (Hyperion 2000, Bruker, Billerica, MA). On each sample, four measurements were carried out and averaged. The measured absorbance of the ATR-FTIR signal depends on the sample surface roughness, especially for samples with cracked surfaces, which leads to a large uncertainty. An example of the location specific measurement result is shown in the SI in Fig. S.1 for two absorbance peaks on a cracked sample after exposure to UV light for 1500 h. Due to the cracks, the measured contour plots for different absorbance peaks are highly non-uniform.

Therefore, on cracked samples, only flat surfaces between the cracks were measured by ATR-FTIR even though the measurements do not represent an average chemical distribution of the whole surface.

## 2.4 ABRASION EXPERIMENTS

### 2.4.1 PARTICLE SIZE DISTRIBUTION OF ABRADED PARTICLES

For the simulation of a sanding or abrasion process, the same set-up was used as described by Schlagenhauf *et al.* [15]. The particle generation was carried out with the Taber Abraser (Model 5135, Taber, North Tonawanda, NY), equipped with the abrasive wheel H-18 (Taber) and 0.75 kg of weight was applied at 60 rpm. The particles were collected through an inlet, mounted on a tube. The air flow was generated with a pump (N816.1.2KN.18, KNF, Germany) and between the Taber Abraser and the pump, either an aerodynamic particle sizer (APS) (Model 3321, TSI, Shoreview, MN) or a scanning mobility particle sizer (SMPS), consisting of a differential mobility analyzer (DMA) equipped with a long DMA column (Model 3080, TSI) and a condensation particle counter (CPC) (Model 3775, TSI), were used to measure the particle size distribution. For imaging, particles were collected on a copper grid with a nanometer aerosol sampler (NAS, modle 3089, TSI) and measured with a transmission electron microscope (TEM, CM30, Philipps, Netherlands).

In order to differentiate particles from the weathered surface and from the unaffected bulk of the samples, the sampling time for one measurement was set to 20 s for both APS and SMPS, and each sample was abraded for 10 min. The first measured particle size distribution of each sample was assumed to represent surface particles and an average of the last ten particle size distributions represented the particles from the bulk sample. For each measurement, three samples were used and averaged.

### 2.4.2 QUANTIFICATION OF EXPOSED MWCNTS

The quantity of exposed MWCNTs in the $PM_1$ fraction of the abraded particles was measured according to the method by Schlagenhauf *et al.* [18] and with manganese ions ($Mn^{2+}$), released by catalyst particles, as indicators for MWCNTs. For each sample, approx. 50 mg of material was abraded (on average approx. 5 µm of the surface), and $PM_1$ particles were collected on Nuclepore track-etch membrane filters (111106, pore size 0.2 µm, Whatman, UK). Particles with aerodynamic diameters above 1 µm were removed by the usage of two cyclones (1031083R, TSI, USA; URG-2000-30EQ, URG, USA; $D_{50}$≈0.9 µm). The filters were immersed in a 0.1 M $HNO_3$ solution (Suprapure Nitric acid 65 %, Merck KGaA, Germany), sonicated for 30 min, and rested for another 30 min. Afterwards, the abraded particles were separated from the solution by centrifuge filtration (Amicon Ultra-4 30kDa, Merck Millipore, Billerica, MA) and the concentration of $Mn^{2+}$ was determined by inductively coupled plasma mass spectrometry (ICP-MS) (Elan 6000, Perkin Elmer, Waltham, MA). For each measurement, five samples were tested and averaged. The quantity of exposed MWCNTs ($X_{MWCNT}$) was determined with Eq. 4

$$X_{MWCNT}(\%) = \frac{m_1}{m_0} \cdot 100\% \quad (4)$$

where $m_1$ is the collected mass of $Mn^{2+}$ and $m_0$ is the maximal collectable mass of $Mn^{2+}$, computed from the known amount of MWCNTs in the abraded sample mass and the release of $Mn^{2+}$ from pure MWCNTs (2.82 µg of $Mn^{2+}$ for 1 mg of MWCNTs).

## 2.5 TOXICITY EXPERIMENTS

### 2.5.1 PARTICLE COLLECTION

The particles for the toxicity tests were generated by abrasion and the usage of the Taber Abrader with the same settings as described in section 2.4.1. The abraded particles then were

collected on Nuclepore track-etch membrane filters without a separation of $PM_1$ and larger particles.

### 2.5.2 CELL CULTURE AND CELL TREATMENT

The human acute monocytic leukemia cell line THP-1 (ATCC: TIP-202) was maintained in RPMI-1640 medium (Sigma-Aldrich) supplemented with 10 % FCS (Lonza), 0.2 mg/ml L-glutamine (Gibco), and 1 % penicillin-streptomycin-neomycin (PSN) (Gibco). Cells were grown at 37 °C in a 5 % $CO_2$ atmosphere, and were sub cultured twice a week. Before each assay, THP-1 monocytes were differentiated into macrophages by adding 200 nM phorbol 12-myristate 13-acetate (PMA) (Fluka) for 3 days. To reasonably disperse abrasion particles, they were suspended in Millipore water containing 0.016 % Pluronic F127 (Sigma) to a final stock solution of 250 µg/ml. The particle suspensions were sonicated in an ultrasonic bath (Bandelin Sonorex Super RK 156 BH) for 10 min and immediately diluted with cell culture medium prior to the experiments.

### 2.5.3 ANALYSIS OF CELL VIABILITY/ACTIVITY (MTS ASSAY)

Cell viability was determined using the CellTiter96 Aqueous One Solution (Promega) containing MTS as the tetrazolium compound according to the manufacturer's instructions. 4 $\times 10^4$ THP-1 cells were seeded in 200 µl of complete cell culture medium per well of a 96 well plate and grown for 3 days in the presence of 200 nM PMA. Differentiated monocytes were then treated with 200 µl per well of different abrasion particles or the positive control $CdSO_4$ at the indicated concentrations for 3 or 24 h. The medium containing particles or $CdSO_4$ was removed and 120 µl of MTS working solution was added for 60 min at 37 °C and 5 % $CO_2$. Optical density was then measured at 490 nm in an EL800 microplate reader (BioTEK Instru-ments). OD(490) values were blank-corrected and normalized to untreated samples.

### 2.5.4 DETECTION OF REACTIVE OXYGEN SPECIES (DCF ASSAY)

The formation of intracellular reactive oxygen species (ROS) was determined using the di-chlorofluorescein (DCF) assay, measuring the conversion of $H_2$DCF (2',7'-dichlodihydrofluorescein, Molecular Probes) to fluorescent DCF by ROS. Briefly, $4 \times 10^4$ THP-1 cells were seeded per well of a 96 well plate in a volume of 200 µl and grown for 3 days in the presence of 200 nM PMA. Thereafter, the medium was replaced by 100 µl of 50 µM $H_2$DCFDA in Hank's buffered salt solution (HBSS) and cells were incubated for 60 min at 37 °C and 5 % $CO_2$. After washing with prewarmed HBSS, cells were exposed to 100 µl of the indicated particle concentrations. The nitrite oxide donor 3-morpholinosydnonimine (Sin-1, Sigma-Aldrich) was used as a positive control. Fluorescent intensities were measured after 2 h using a FLX800 fluorescence microplate reader (BioTEK Instruments, Winooski, VT) at an excitation wavelength of 485 nm and an emission wavelength of 528 nm. Fluorescence values were blank-corrected and normalized to untreated controls.

### 2.6 Statistical analysis

The significance of difference between different datasets was measured with *F*-tests by usage of one-way analysis of variance (ANOVA) (OriginPro 8, OriginLab Corporation, USA).

The toxicity data are shown as mean ± standard error of the mean (StEM) from at least three independent experiments. Statistical significance was determined using a two-tailed Student's t test (Microsoft Excel, Microsoft Corporation, USA). A p-value below 0.05 was considered to be statistically significant.

## 3. RESULTS AND DISCUSSION

### 3.1 WATER UPTAKE KINETICS

The weight increase of the water bath samples is shown in Fig. 1(a). The sample with 0.1 wt% MWCNTs showed the fastest uptake of water under all three temperature conditions, although the maximum uptake values of the two nanocomposites could not be statistically differentiated. Further, both nanocomposites had a higher uptake capacity than the neat epoxy. Independent of the temperature, they had a maximum weight increase of 3.2 %, while the epoxy showed a significantly lower weight increase of 2.9 % ($p<0.005$ for the 70 °C samples).

The different water uptake equilibriums of the neat epoxy and the composites can be explained by a change of the available free volume and the number of open hydrogen bonds [40] in the epoxy matrix. The free volume is the volume of the bulk material that is not actually occupied by the polymer molecules themselves [41]. Due to the incorporation of MWCNTs, the free volume of the epoxy could have been changed by the creation of additional voids in MWCNT agglomerates and in the interfacial regions between MWCNTs and the epoxy. Further, it is known, that CNTs can influence the curing behavior of the epoxy [42] and thus lead to a change in the molecular packing and segmental mobility that influences the free volume directly. Since the amount of added MWCNTs has no notable influence on the equilibrium water uptake in the present study, we hypothesize that the obtained results could be caused by a change in the curing behavior.

The calculated diffusion coefficients and activation energies were compared to reference data, obtained from studies with different epoxy systems, and are shown in Fig. 1(b) and Fig. 1(c). As indicated by the uptake rates in Fig. 1(a), the sample with 0.1 wt% shows the highest diffusion coefficients while the other two samples show similar results. The activation energy of the 1 wt% sample is significant smaller than for the other samples, but this result can be caused by the low number of fitted points in Fig. 1(b). The measured diffusion coefficients and activation energies of all samples lie in the upper part of the ranges reported by other studies, indicating that the used epoxy was comparable with other epoxy systems.

The diffusion coefficient is mainly influenced by the free volume [40], but when a nanofiller is added to a polymer, the filler also can act as a diffusion barrier [4]. The testing results indicate that the sample with 0.1 wt% shows a higher diffusion coefficient than the neat epoxy due to the increased free volume, proven by the higher equilibrium water uptake, and also a higher diffusion coefficient than the 1 wt% sample due to the lower diffusion barrier.

The studies in the literature show conflicting results regarding the effects of the CNT addition on the water uptake compared to the epoxy matrix; the values of the equilibrium weight gain and diffusion coefficient could increase or decrease[4, 40, 43, 44] (See Table S.2 in the SI for a summary of the results). It seems the effect depends on the specific system and no general trend is observed.

## 3.2 WEATHERING IMPACT ON THE SAMPLE SURFACE

### 3.2.1 SURFACE CHEMISTRY

The surface chemistry and its changes due to weathering have been characterized by ATR-FTIR, the results of the samples with 1 wt% MWCNTs, compared to an untreated sample, are shown in Fig. 2(a). The same spectrum with the results of the neat epoxy can be found in the SI (Fig. S.2). Both samples in Fig. 2(a) underwent the weathering process for 1000 h and the figures include dashed lines that mark the identified peaks, given in Table S.3. Both presented weathering processes were conducted at elevated temperatures. To identify temperature effects on the surface chemistry, also weathering at elevated temperatures, low RH, and no light was carried out, presented in the SI in Section 4.

For all ATR-FTIR measurements, no difference between the neat epoxy samples and the composite, undergoing the same weathering treatment, was measured, but the weathering treatments had different impacts on the results. Immersion in a water bath at 70 °C had no effect on the surface chemistry. The exposure to UV light induced changes for all detected

peaks. In the range between 1850 $cm^{-1}$ and 1500 $cm^{-1}$, a new peak was formed that mainly consisted of a combination of two peaks at 1735 $cm^{-1}$ and at 1650 $cm^{-1}$, that can be assigned to carbonyl groups. The formation of this peak has been detected also in other publications [45–49]. At 827 $cm^{-1}$, the absorbance of the aromatic C-H out of plane vibration decreased significantly by the exposure to the UV light. For a proper comparison of the neat epoxy and the nanocomposite, a plot with the differences between the measured graphs would be useful, as presented by Petersen *et al.*[49]. But normalization with a reference peak for the present samples was not possible because the UV degradation caused an intensity alteration for all measured absorbance peaks.

To show the impact of the exposure time of UV light on the surface chemistry, an ATR-FTIR time series is shown in Fig. 2(b) for the neat epoxy samples and the 1 wt% MWCNT/epoxy nanocomposites. A closer look at the region between 1800 $cm^{-1}$ and 1550 $cm^{-1}$ reveals that between 500 h and 1000 h a quasi-stable state of the surface chemistry was reached. For both samples, a change of the surface chemistry can be noticed for the samples with an exposure time of 1500 h where a lower degree of degradation is measured compared to the 1000 h sample, which was attributed to surface fall-off detailed in the next section.

### 3.2.2 TOPOGRAPHY CHANGE

The topography changes, caused by the weathering processes, were examined with SEM and AFM. For the water bath samples, no changes of the surface topography were detected, as shown in Fig. 3(a). For the UV light samples, visible cracks on the sample surface were formed between 750 h and 1000 h of exposure time for both samples, the neat epoxy and the 1 wt% MWCNT/epoxy nanocomposite. After 1500 h exposure to UV light, the samples were crisscrossed by many micro cracks as shown in Fig. 3(b). Besides the cracks, it is also visible that the samples had regions with a relatively flat surface, speckled by islands with a rough surface, as shown in Fig. 3(b) and Fig. 3(c). The islands were also characterized by AFM

(Fig. 3(d)), the measured island step sizes ranged between 2.25 µm and 2.85 µm. In addition to the changes in the micrometer range, the UV light exposure also damaged the surface at the nano scale, shown in Fig. 3(e). After 1000 h of degradation, cavities appeared on the surface. No MWCNTs were detected on the surfaces after all exposure durations, neither by SEM nor by AFM.

While the water bath samples did not show any measurable effects from the weathering process, the exposure to UV light caused changes in the surface chemistry, measured by ATR-FTIR, and in the topography, measured with SEM and AFM. Despite the measured degradation, no MWCNTs were detected on the surface of the samples. This can be explained first by the applied energy dose of the UV light which was lower compared to other studies [32, 49], and secondly by a delamination of the top surface layer implied by the results of the ATR-FTIR and the topography measurements.

The results of the SEM and AFM imaging showed that islands remained on the surface after the exposure to UV light for 1500 h. The rough surface of the islands, shown in Fig. 3(c), indicated that they were exposed to the UV light for a longer time than the smooth surroundings and it can be inferred that the surface layer above the smooth surface fell off after a certain exposure time. This result is corroborated by the time series of the ATR-FTIR measurements in Fig. 2(b). Between the exposure to 1000 and 1500 h, a decrease of the surface degradation was observed, indicating that between those two measurements a large part of the surface was delaminated and removed from the sample.

The UV light degrades the polymer and may lead to loss of the matrix material on the surface, thus exposing CNTs and leaving an apparent CNT network on the degraded surface [19, 27, 32, 47, 49]. In our case, it seemed the surface delamination and fall-off happened before the MWCNTs were exposed on the surface, thus reducing the possibility of release of free standing MWCNTs into the environment. This result is different from former studies where the

formation of CNT networks was observed [19, 27, 32, 47, 49]. A comparison of the weathering conditions for the compared studies is given in Table 1.

The differences among the studies are the used matrix material, the sample thickness, the CNT load, the applied RH, and the temperature during the UV light exposure. The influence of the matrix material can be excluded as most studies were conducted with epoxy composites, also the CNT load seems to play a minor role as CNT networks were observed for different samples with CNT loads from 0.72 wt% to 3.5%. The thickness of the used samples in this study is much larger than those in similar studies. During the degradation process by UV light, only a thin surface layer is degrading and shrinking while the bulk remains unaffected. This situation induces stress on the surface leading to cracks. It can be hypothesized that due to the larger sample thickness, the samples in this study provided stronger resistance to the deformation on the surface which resulted in larger stress and more cracks. Another factor that could have contributed to the delamination of the surface layer is the applied humidity during the UV exposure. Compared to the other studies with epoxy composites, the used RH in this study was low, causing a low content of adsorbed water in the samples. It already has been shown by several studies, that the absorption of water in epoxy can cause a decrease of the glass transition temperature $T_g$ of 25 to 30°C to values below the applied temperatures during the UV exposure experiments [21, 50, 51]. Therefore the epoxy matrix in those studies could have been less brittle than our samples. Due to the lower stiffness, less stress would be induced on the surface and the polymer could reduce the stress by relaxation processes.

## 3.3 IMPACT OF WEATHERING ON THE PARTICLE RELEASE

### 3.3.1 ABRASION OF WEATHERED SAMPLES

The particle size distributions of abraded particles from neat epoxy and 1 wt% MWCNT samples that underwent different weathering treatments were determined. Each sample showed three particle size modes. Mode 1 was measured in the nano range by SMPS and mode 2 & 3 in the micro range by APS. The peak maxima of all measured distributions are given in the SI in Table S.4.

The particle size distributions from the SMPS measurements are shown in Fig. 4(a). In the nano range, no difference between the particles from the surface and the bulk was detected. Also the difference between the neat epoxy and the nanocomposite samples was small and lay within the measurement error. The water bath treatment had no impact on the particle size, but for the UV light exposed samples, a slight increase of the particle size was measurable. The peaks increased by about 30 nm for both samples with an exposure time of 1500 h.

In the micro range, a clear difference in the measured particle size distributions between the abraded particles from the surface in Fig. 4(b) and the bulk in Fig. 4(c) is visible. For the surface particles, mode 3 that ranges between 1 and 2.6 μm was more dominant than mode 2 (0.6 – 1 μm); for the bulk particles, it was the opposite. For the surface particles, the results showed significant variations among the samples with the same treatment, expressed by the large error bars for some measurements. For the bulk particles, the results are more homogeneous among the samples, and the difference between the neat epoxy and the nanocomposite was moderate.

With consideration of the large error bars, the particle size distributions of the surface particles are comparable for all measurements. No evolvement of the distributions is clearly related to the weathering processes, except that the samples exposed to UV light for 1500 h released almost exclusively particles with diameters below 5 μm. This could be an indication that the UV light exposure did cause a change of brittleness of the sample surface or that the formed micro cracks had an influence on the measured particle size. The bulk particles

showed no difference between the untreated samples and the water bath samples. For the UV light degraded samples, it is noticeable that mode 3 was more dominant compared to the untreated samples. This result was repeatable for all measurements even though it was assumed that the abraded particles from the bulk were not affected by the UV light due to its low penetration depth [52].

The collected particles on TEM grids showed similar behavior for the weathered samples compared to abraded particles from untreated MWCNT/epoxy nanocomposites [15,53]. Both TEM images in Fig. 4(d) show abraded particles from a sample exposed to UV light for 1500 h. The first image shows a short fiber that possibly originated from a chopped MWCNT since the diameter is similar to the used MWCNTs. This is the only free standing fiber found on all samples, so an enhanced release of free MWCNTs, caused by the weathering processes, can be neglected. The second TEM image shows a particle with several protruding MWCNTs.

### 3.3.2 QUANTIFICATION OF EXPOSED CNTS

The quantity of exposed MWCNTs in the $PM_1$ fraction of the abraded particles from the samples (approx. 5 µm depth) is shown in Fig. 5. The release fractions of all four degradation scenarios remained within the standard deviation of the untreated samples and thus no significant increase of exposed MWCNTs was caused by the weathering processes. The samples exposed to UV light for 500 h showed a MWCNT release fraction of approx. 0.6%, which was 50% higher compared to the samples with exposure times of 1000 and 1500 h (approx. 0.4 %; significance $p < 0.001$). The water bath samples showed the lowest release of exposed MWCNTs (approx. 0.3 %). The differences among UV light degraded samples can be explained partially by the measured particle size distributions from the bulk measurements. Fig. 4(c) shows that the fraction of particles bigger than 1 µm, compared to the fraction of $PM_1$ particles, increased with longer UV exposure time and thus less $PM_1$ particles were collected for samples with long exposure times. The large error bars for the release of exposed

MWCNTs from the untreated sample do not allow an extensive comparison with the results from the weathered samples. However, it can be concluded that the weathering processes did not cause a significantly higher release of exposed MWCNTs and therefore the exposure risk was not increased.

For samples with much more surface degradation, e.g. presented by Nguyen *et al.* [19] where apparently several hundred nm of the surface were removed during the exposure to UV light, the quantification experiment may be able to identify an increase of the exposed MWCNTs. However, for commercial products with included UV stabilizers, the occurrence of such strongly degraded surfaces is going to be quite uncommon.

### 3.4 CYTOTOXICOLOGICAL ASSESSMENT

In addition to studying if aging alters the abrasion properties of CNT/epoxy composites, it is important to understand if abraded particles from such composites can elicit adverse human health effects. A significant induction of ROS and/or a slight decrease in cell viability has been described for several cell types that were exposed to MWCNTs *in vitro* [34, 54–57]. In a previous study we have confirmed that such adverse effects were also induced in THP-1 cells with the same MWCNTs as used in this work [18]. Similar to pure MWCNTs, abraded particles from untreated and aged MWCNT composites induced a time- and concentration-dependent decrease in cell viability as measured by the MTS assay (Fig. 6(a)). The cell activity was always above 70 % even at the highest concentration of 80 µg/ml of abraded particles, which represents the scenario for a high single-dose occupational exposure. Particles abraded from MWCNT composites that were treated with UV light for 1500 h or were kept in the water bath for 1000 h did not show any additional toxicity as compared to non-aged control particles.

To investigate if the observed slight cytotoxicity was due to exposed MWCNTs we also analyzed the effects of particles abraded from untreated or aged epoxy that did not contain any MWCNTs. Interestingly, a very similar decrease in THP-1 viability was observed, suggesting that this adverse effect was induced by the epoxy particles. Another source of cytotoxic material may be the released particles from the abrasion wheel but this was excluded already in our previous study [18].

In contrast to pristine MWCNTs, all abraded particles from untreated or aged samples with or without MWCNTs did not induce the formation of ROS in the DCF-assay (Fig. 6(b)). The positive control Sin-1 (a morpholino compound) confirmed that the assay was sensitive to detect intracellular free radicals. Therefore, the observed decrease in cell viability was not due to the formation of ROS. As oxidative stress is assumed to be a major factor in CNT induced cell death, the observed absence of ROS further supports our hypothesis that the cytotoxic effects on THP-1 cells were due to the epoxy particles rather than from exposed MWCNTs. Although CNTs are a diverse population of materials, it appears that a common mechanism may be responsible for driving CNT toxicity [24]. According to the proposed ROS paradigm, the induction of ROS by CNTs may result in oxidative damage to cellular components, inflammatory responses and ultimately lead to cell death. Whether and to which extent these adverse effects are occurring is strongly dependent on CNT length, rigidity, metal content, tendency to aggregate/agglomerate and surface chemistry, among others. In a previous study we have tested the cytotoxicity of abraded particles containing free-standing MWCNTs [18]. Neither pure MWCNTs nor abraded particles containing a low amount of exposed MWCNTs induced the release of inflammatory cytokines (IL-8 or TNFα) or DNA strand breaks in THP-1 cells. The reason why we did not observe any adverse inflammatory responses or genotoxic effects even with pure MWCNTs was most likely that the MWCNTs used were rather short. Indeed, especially long, needle-like MWCNTs have been described to induce significant

adverse effects both *in vitro* and *in vivo* such as radical formation, inflammation, fibrosis and mesothelioma [58–60]. Therefore, we decided not to test the inflammatory and genotoxic effects of our aged nanocomposites, which did not show any additional release of exposed MWCNTs upon abrasion. In fact, complex endpoints involving the interplay of many different cell types such as inflammatory responses may not be well predicted in our simple *in vitro* model. Our study focused on acute toxicity tests, and intended to investigate the risk of a single-dose occupational exposure during mechanical abrasion of a fresh or weathered MWCNT composite material. Chronic studies in more complex co-culture or *in vivo* models [61–63] would be required to assess the effects of exposure to particles released by long term weathering and degradation of nanocomposite.

## 4. CONCLUSION

Compared to other weathering studies with CNT/epoxy nanocomposites, our study investigated not only UV degradation but also the aging by immersion in water in order to detect a possible release of the nanofiller. The measurements of the water uptake showed that the MWCNTs had an influence on both the equilibrium uptake capacity and the uptake kinetics. No notable influence by the weathering process on the surface chemistry, the particle size of abraded particles, and the particle cytotoxicity was detected.

Our results from the degradation process by exposure to UV light were different compared to similar studies where no delamination of the top surface layer was observed. This effect had the consequence that after 1500 h of exposure, the surface was relatively smooth and showed a low degree of chemical degradation. For longer exposure times, the formation of a MWCNT network on the surface, as shown by other studies, cannot be ruled out. Further, a several-µm-thick layer below the surface of the nanocomposite was affected by the exposure to UV light, causing a release of larger particles compared to the untreated sample when an abrasion process was applied, and thus a release of a smaller quantity of exposed MWCNTs in the $PM_1$

fraction. This result can change if samples with a formed network of MWCNTs on the surface are abraded.

With the presented dataset, it is possible to estimate the risk for an acute exposure to abraded particles of the investigated MWCNT/epoxy nanocomposites. We were able to determine the dose of exposed MWCNTs when the abrasion process was applied and also to evaluate the toxicity of the particles. With the obtained results, we can conclude that the health risk upon inhalation of the abraded particles is low for a single exposure event. The risk for long term exposures cannot be estimated with the obtained results.

## 5. ACKNOWLEDGMENTS

This study was financed by the Swiss National Science Foundation (NFP 64), "Evaluation platform for safety and environment risks of carbon nanotube reinforced nanocomposites", 406440_131286. We appreciate the availability of the Scanning Probe Microscopy User Lab at Empa for the AFM measurements.

## 6. REFERENCES


1 R. Hollertz, S. Chatterjee, H. Gutmann, T. Geiger, F. A. Nüesch and B. T. T. Chu, *Nanotechnology*, 2011, **22**, 125702.

2 A. B. Sulong, J. Park, N. Lee and J. Goak, *J. Compos. Mater.*, 2006, **40**, 1947–1960.

3 D. S. Lim, J. W. An and H. J. Lee, *Wear*, 2002, **252**, 512–517.

4 L. Guadagno, L. Vertuccio, A. Sorrentino, M. Raimondo, C. Naddeo, V. Vittoria, G. Iannuzzo, E. Calvi and S. Russo, *Carbon N. Y.*, 2009, **47**, 2419–2430.

5 T. Kashiwagi, E. Grulke, J. Hilding, R. Harris, W. Awad and J. Douglas, *Macromol. Rapid Commun.*, 2002, **23**, 761–765.

6 B. Schartel, P. Pötschke, U. Knoll and M. Abdel-Goad, *Eur. Polym. J.*, 2005, **41**, 1061–1070.

7 H. Huang, C. H. Liu, Y. Wu and S. Fan, *Adv. Mater.*, 2005, **17**, 1652–1656.

8 Y. S. Song and J. R. Youn, *Carbon N. Y.*, 2005, **43**, 1378–1385.

9 C. Kingston, R. Zepp, A. Andrady, D. Boverhof, R. Fehir, D. Hawkins, J. Roberts, P. Sayre, B. Shelton, Y. Sultan, V. Vejins and W. Wohlleben, *Carbon N. Y.*, 2013, **68**, 33–57.

10 J. Du, S. Wang, H. You and X. Zhao, *Environ. Toxicol. Pharmacol.*, 2013, **36**, 451–462.

11 A. Erdely, M. Dahm, B. T. Chen, P. C. Zeidler-Erdely, J. E. Fernback, M. E. Birch, D. E. Evans, M. L. Kashon, J. A. Deddens, T. Hulderman, S. A. Bilgesu, L. Battelli, D. Schwegler-Berry, H. D. Leonard, W. McKinney, D. G. Frazer, J. M. Antonini, D. W. Porter, V. Castranova and M. K. Schubauer-Berigan, *Part. Fibre Toxicol.*, 2013, **10**.

12 J. P. Kaiser, M. Roesslein, T. Buerki-Thurnherr and P. Wick, *Curr. Med. Chem.*, 2011, **18**, 2115–2128.

13 B. Nowack, R. M. David, H. Fissan, H. Morris, J. A. Shatkin, M. Stintz, R. Zepp, D. Brouwer and J. Anne, *Environ. Int.*, 2013, **59**, 1–11.

14 L. Schlagenhauf, F. Nüesch and J. Wang, *Fibers*, 2014, **2**, 108–127.

15 L. Schlagenhauf, B. T. T. Chu, J. Buha, F. Nüesch and J. Wang, *Environ. Sci. Technol.*, 2012, **46**, 7366–7372.

16 G. Huang, J. Park, L. Cena, B. Shelton and T. Peters, *J. Nanoparticle Res.*, 2012, **14**, 1231.

17 L. Golanski, A. Guiot, M. Pras, M. Malarde and F. Tardif, *J. Nanoparticle Res.*, 2012, **14**.

18 L. Schlagenhauf, T. Buerki-Thurnherr, Y.-Y. Kuo, A. Wichser, F. Nüesch, P. Wick and J. Wang, *Environ. Sci. Technol.*, 2015, DOI: 10.1021/acs.est.5b02750.

19 T. Nguyen, B. Pellegrin, C. Bernard, X. Gu, J. M. Gorham, P. Stutzman, D. Stanley, A. Shapiro, E. Byrd, R. Hettenhouser and J. Chin, *J. Phys. Conf. Ser.*, 2011, **304**, 12060.

20 S. Hirth, L. Cena, G. Cox, Z. Tomović, T. Peters and W. Wohlleben, *J. Nanoparticle Res.*, 2013, **15**, 1504.

21 B. Deneve and M. E. R. Shanahan, *Polymer (Guildf).*, 1993, **34**, 5099–5105.

22 G. Z. Xiao and M. E. R. Shanahan, *Polymer (Guildf).*, 1998, **39**, 3253–3260.

23 M. Y. M. Chiang and M. Fernandez-Garcia, *J. Appl. Polym. Sci.*, 2003, **87**, 1436–1444.

24 H. J. Johnston, G. R. Hutchison, F. M. Christensen, S. Peters, S. Hankin, K. Aschberger and V. Stone, *Nanotoxicology*, 2010, **4**, 207–46.

25 K. Donaldson, C. A. Poland, F. A. Murphy, M. MacFarlane, T. Chernova and A. Schinwald, *Adv. Drug Deliv. Rev.*, 2013, **65**, 2078–86.

26 L. Wang, T. A. Stueckle, A. Mishra, R. Derk, T. Meighan, V. Castranova and Y. Rojanasakul, *Nanotoxicology*, 2014, **8**, 485–507.

27 J. Ging, R. Tejerina-Anton, G. Ramakrishnan, M. Nielsen, K. Murphy, J. M. Gorham, T. Nguyen and A. Orlov, *Sci. Total Environ.*, 2014, **473-474**, 9–19.

28 L. Mikkelsen, K. A. Jensen, I. K. Koponen, A. T. Saber, H. Wallin, S. Loft, U. Vogel and P. Møller, *Nanotoxicology*, 2013, **7**, 117–34.

29 A. T. Saber, N. R. Jacobsen, A. Mortensen, J. Szarek, P. Jackson, A. M. Madsen, K. A. Jensen, I. K. Koponen, G. Brunborg, K. B. Gutzkow, U. Vogel and H. Wallin, *Part. Fibre Toxicol.*, 2012, **9**.

30 A. T. Saber, I. K. Koponen, K. A. Jensen, N. R. Jacobsen, L. Mikkelsen, P. Møller, S.Loft, U. Vogel, H. H. Wallin and P. Moller, *Nanotoxicology*, 2012, **6**, 776–788.

31 W. Wohlleben, S. Brill, M. W. Meier, M. Mertler, G. Cox, S. Hirth, B. von Vacano, V. Strauss, S. Treumann, K. Wiench, L. Ma-Hock and R. Landsiedel, *Small*, 2011, **7**, 2384–2395.

32 W. Wohlleben, M. W. Meier, S. Vogel, R. Landsiedel, G. Cox, S. Hirth, Z. Tomovic and Ž. Tomović, *Nanoscale*, 2013, **5**, 369–380.

33 Bayer Material Science (2012). Product Information Baytubes C150p. Retrieved from http://www.baytubes.com/product_production/baytubes_data.html.

34 Thurnherr, T.; Su D. S.; Diener L.; Weinberg G.; Manser P.; Pfänder N.; Arrigo R.; Schuster M. E.; Wick P.; Krug H. F. (2009) *Nanotoxicology*, 3(4): 319–338.

35 Wang, J., Bahk, Y.K., Chen, S-C., Pui, D.Y.H. (2015) *Carbon*, 93, 441–450, DOI: 10.1016/j.carbon.2015.05.079.

36 Zybex technologies (2014) Safety Data Sheet ZNT-boost (Solid). Retrieved from http://www.zyvextech.com/assets/pdf/ZNT-bOOST-SOLID-Resin-Linear-Polymer-20032514-3.pdf.

37 Ma, P. C.; Siddiqui, N. A.; Marom, G.; Kim, J. K. (2010) *Composites: Part A*, 41, 1345.

38 W. Liu, S. V. V Hoa and M. Pugh, *Compos. Sci. Technol.*, 2007, **67**, 3308–3315.

39 W. Liu, S. V Hoa and M. Pugh, *Compos. Sci. Technol.*, 2008, **68**, 2066–2072.

40 O. Starkova, S. T. Buschhorn, E. Mannov, K. Schulte and A. Aniskevich, *Eur. Polym. J.*, 2013, **49**, 2138–2148.

41 G. Choudalakis and a. D. D. Gotsis, *Curr. Opin. Colloid Interface Sci.*, 2012, **17**, 132–140.

42 A. Allaoui and N. El Bounia, *Express Polym. Lett.*, 2009, **3**, 588–594.

43 N. M. Barkoula, A. Paipetis, T. Matikas, A. Vavouliotis, P. Karapappas and V. Kostopoulos, *Mech. Compos. Mater.*, 2009, **45**, 21–32.

44 S. G. G. Prolongo, M. R. R. Gude and A. Ureña, *Compos. Part A Appl. Sci. Manuf.*, 2012, **43**, 2169–2175.

45 G. Zhang, W. G. Pitt, S. R. Goates and N. L. Owen, *J. Appl. Polym. Sci.*, 1994, **54**, 419–427.

46 N. Mailhot, S. Morlat-Theias, M. Ouahioune and J. L. Gardette, *Macromol. Chem. Phys.*, 2005, **206**, 575–584.

47 T. Nguyen, B. Pellegrin, L. Mermet, A. Shapiro, X. Gu and J. Chin, in *Nanotechnology 2009: Fabrication, Particles, Characterization, MEMS, Electronics and Photonics - Technical Proceedings of the 2009 NSTI Nanotechnology Confer*, 2009, vol. 1, pp. 90–93.

48 J. M. Gorham, T. Nguyen, C. Bernard, D. Stanley and R. David Holbrook, *Surf. Interface Anal.*, 2012, **44**, 1572–1581.

49 E. J. Petersen, T. Lam, J. M. Gorham, K. C. Scott, C. J. Long, D. Stanley, R. Sharma, J. Alexander Liddle, B. Pellegrin and T. Nguyen, *Carbon N. Y.*, 2014, **69**, 194–205.

50 C. Zou, J. C. Fothergill and S. W. Rowe, *Ieee Trans. Dielectr. Electr. Insul.*, 2008, **15**, 106–117.

51 M. Fernández-García, M. Y. M. Chiang and M. Fernandez-Garcia, *J. Appl. Polym. Sci.*, 2002, **84**, 1581–1591.

52 R. Zhang, X. Gu, H. Chen, J. Zhang, Y. Li, T. Nguyen, T. C. Sandreczki and Y. C. Jean, *J. Polym. Sci. Part B Polym. Phys.*, 2004, **42**, 2441–2459.

53 D. Bello, B. L. Wardle, N. Yamamoto, R. G. DeVilloria and M. Hallock, in *ICCM17 proceedings*, 2011.

54 T. Thurnherr, C. Brandenberger, K. Fischer, L. Diener, P. Manser, X. Maeder-Althaus, J.-P. Kaiser, H. F. Krug, B. Rothen-Rutishauser and P. Wick, *Toxicol. Lett.*, 2011, **200**, 176–186.

55 S.-F. Ye, Y.-H. Wu, Z.-Q. Hou and Q.-Q. Zhang, *Biochem. Biophys. Res. Commun.*, 2009, **379**, 643–8.

56 G. Visalli, M. P. Bertuccio, D. Iannazzo, A. Piperno, A. Pistone and A. Di Pietro, *Toxicol. In Vitro*, 2014, **29**, 352–362.

57 B. Rothen-Rutishauser, D. M. Brown, M. Piallier-Boyles, I. A. Kinloch, A. H. Windle, P. Gehr and V. Stone, *Nanotoxicology*, 2010, **4**, 331–42.

58 F. A. Murphy, C. A. Poland, R. Duffin and K. Donaldson, *Nanotoxicology*, 2013, **7**, 1157–67.

59 P. Nymark, K. A. Jensen, S. Suhonen, Y. Kembouche, M. Vippola, J. Kleinjans, J. Catalán, H. Norppa, J. van Delft and J. J. Briedé, *Part. Fibre Toxicol.*, 2014, **11**, 4.

60 J. Palomäki, E. Välimäki, J. Sund, M. Vippola, P. A. Clausen, K. A. Jensen, K. Savolainen, S. Matikainen and H. Alenius, *ACS Nano*, 2011, **5**, 6861–6870.

61 L. Müller, M. Riediker, P. Wick, M. Mohr, P. Gehr, B. Rothen-Rutishauser and L. Muller, *J. R. Soc. Interface*, 2010, **7**, S27–S40.

62 M. Gasser, P. Wick, M. J. D. Clift, F. Blank, L. Diener, B. Yan, P. Gehr, H. F. Krug and B. Rothen-Rutishauser, *Part. Fibre Toxicol.*, 2012, **9**, 17.

63 D. van Berlo, V. Wilhelmi, A. W. Boots, M. Hullmann, T. A. J. Kuhlbusch, A. Bast, R. P. F. Schins and C. Albrecht, *Arch. Toxicol.*, 2014, **88**, 1725–1737.

631 Tab. 1 Comparison of different UV light weathering studies on CNT/polymer nanocomposites

| Study | Matrix material | Sample thickness | CNT load | RH | Temperature |
|---|---|---|---|---|---|
| Nguyen *et al.*[42] | Epoxy | 0.125 mm | 0.72 wt% | 75 % | 50 °C |
| Nguyen *et al.*[19] | Epoxy | 0.15 mm | 0.72 wt% | 75 % | 50 °C |
| Wohlleben *et al.*[32] | Polyurethane | 1.5 and 2 mm | 3 wt% | Low RH or 50 % | 65 °C |
| Ging *et al*[27]. | Epoxy | 0.4 mm | 1 wt% | 75 % | 30 °C |
| Petersen *et al.*[44] | Epoxy | 0.15 mm | 3.5 wt% | 75 % | 50 °C |
| This study | Epoxy | 4 mm | 1 wt% | ≤ 5 % | 60 °C |

632

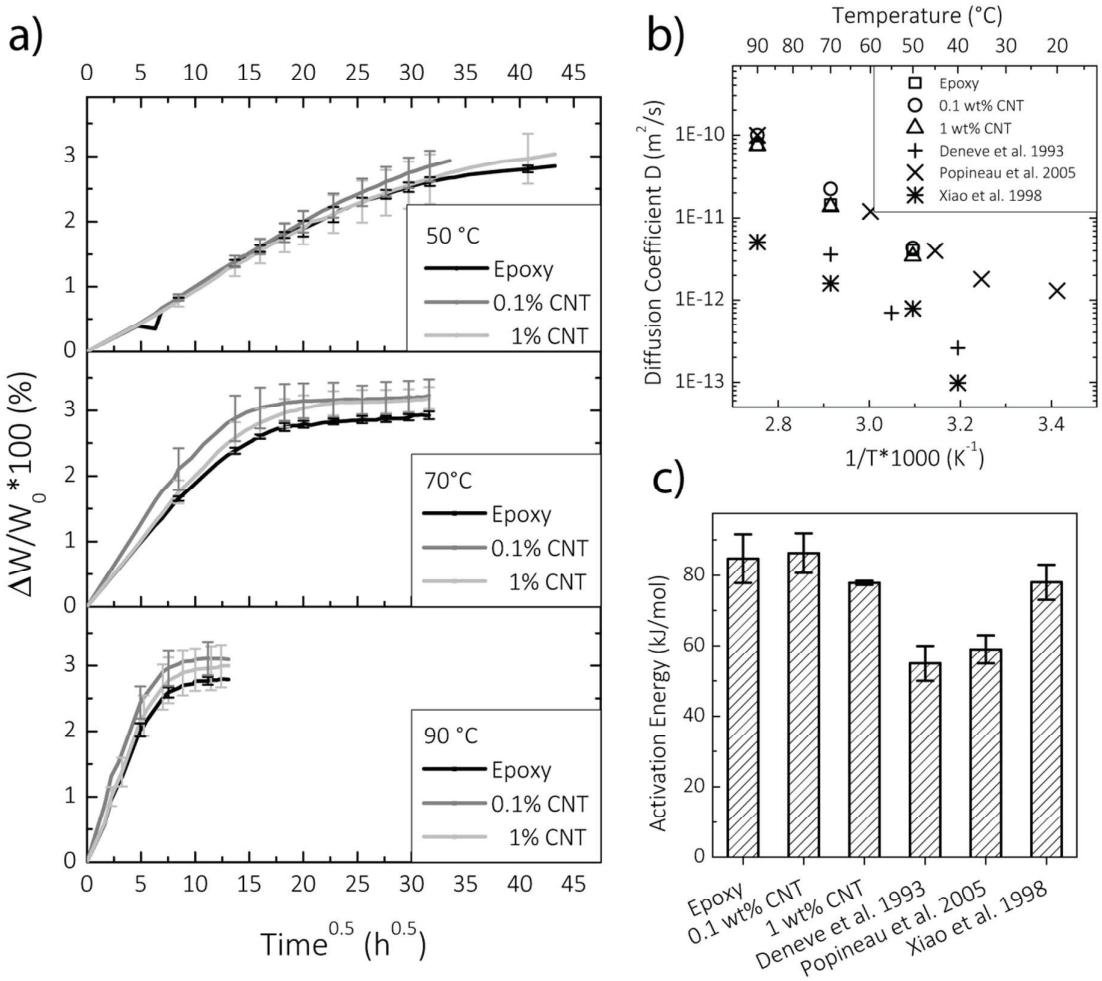


633

634 Figure 1: a) Weight increases in the water bath for the three samples at different temperatures.
635 b) Arrhenius plot of the obtained diffusion coefficients compared to reference data. c)
636 Activation energies of the water uptake compared to reference data from studies with other
637 epoxy systems.

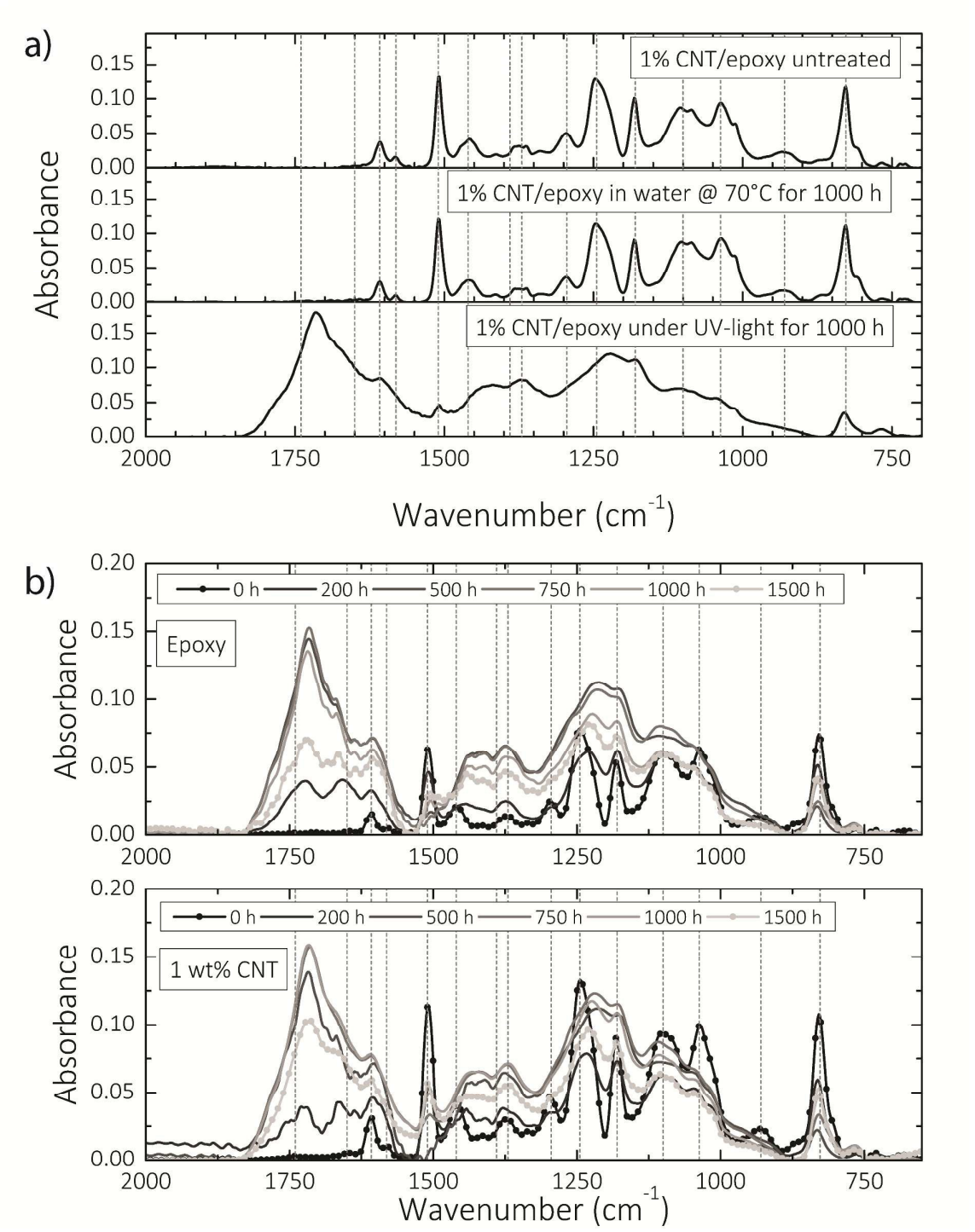


Figure 2: a) ATF-FTIR measurements of the samples after 1000 h of weathering compared to untreated samples for the 1 wt% MWCNT/epoxy samples. The vertical lines indicate the identified peaks; a table with all identified peaks is given in the SI (Tab.S.2). b) Time series of the impact of the UV light on the surface chemistry for a neat epoxy (top) and a 1 wt% MWCNT/epoxy nanocomposite (bottom).

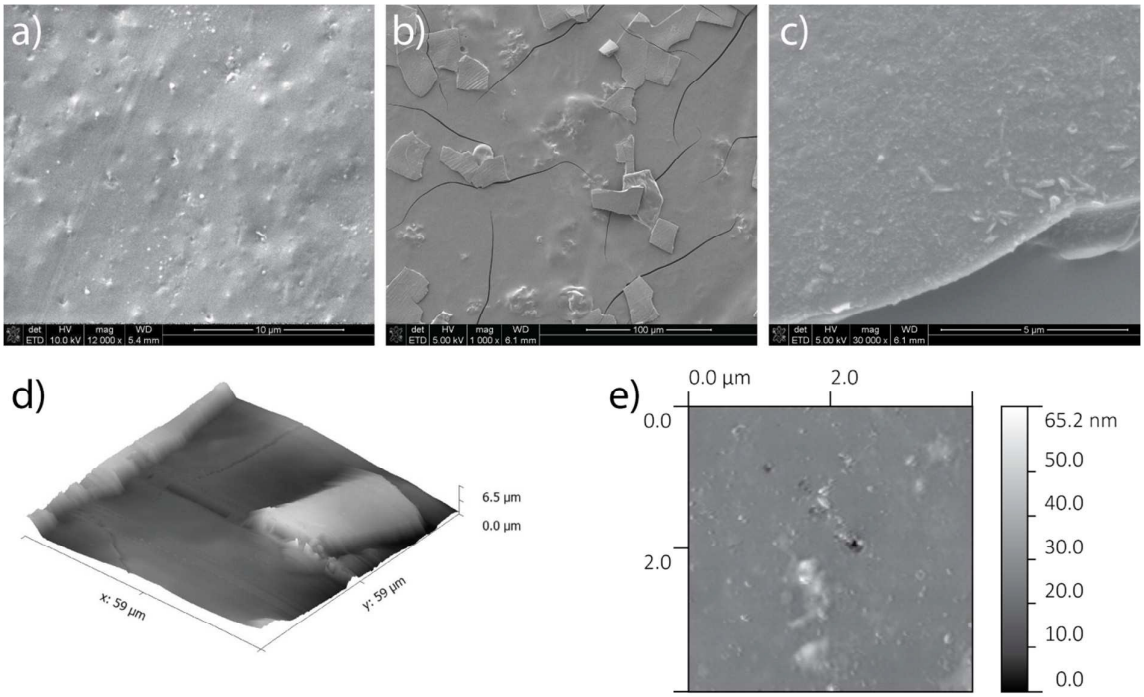


644

645 Figure 3: a) SEM image of a 1 wt% MWCNT/epoxy sample that was immersed in water at
646 70 °C for 1000 h; b) & c) SEM images of a 1 wt% MWCNT/epoxy sample after exposure to
647 UV light for 1500 h. d) AFM image of a remained particle of the top surface layer after
648 1500 h of UV light exposure e) AFM image of the implied damage on the surface after 1000 h
649 of UV light exposure.

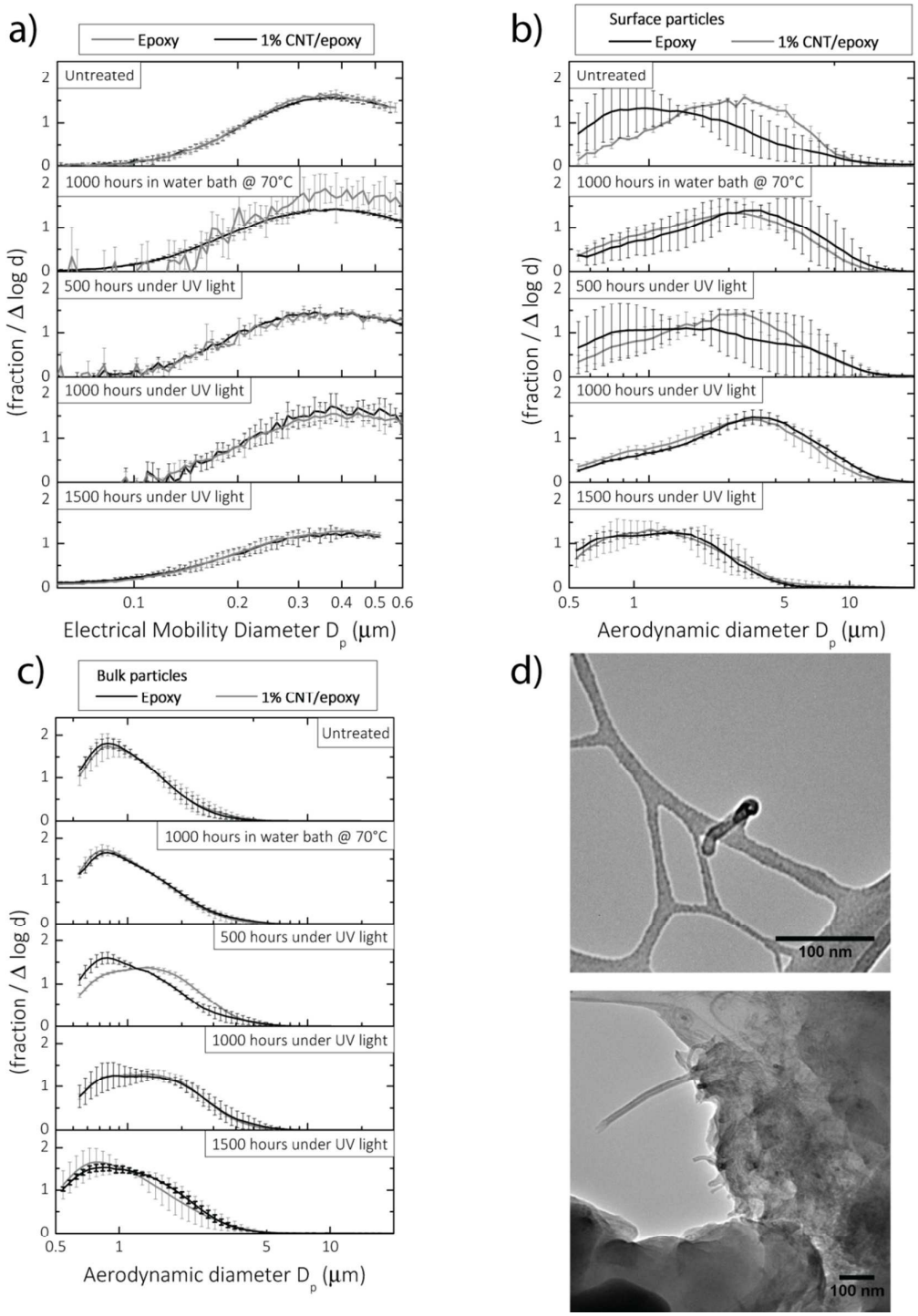


Figure 4: a) Particle size distributions in the nano range of the abraded particles from the weathering samples. b) & c) Particle size distributions in the micro range of the abraded particles from the weathering samples, b) from surface particles and c) from bulk particles. d) TEM images of abraded particles from a 1 wt% MWCNT/epoxy sample after 1500 h under UV light, top: a chopped and free standing MWCNT, bottom: a protruding MWCNT from an agglomerate of MWCNTs inside of a particle

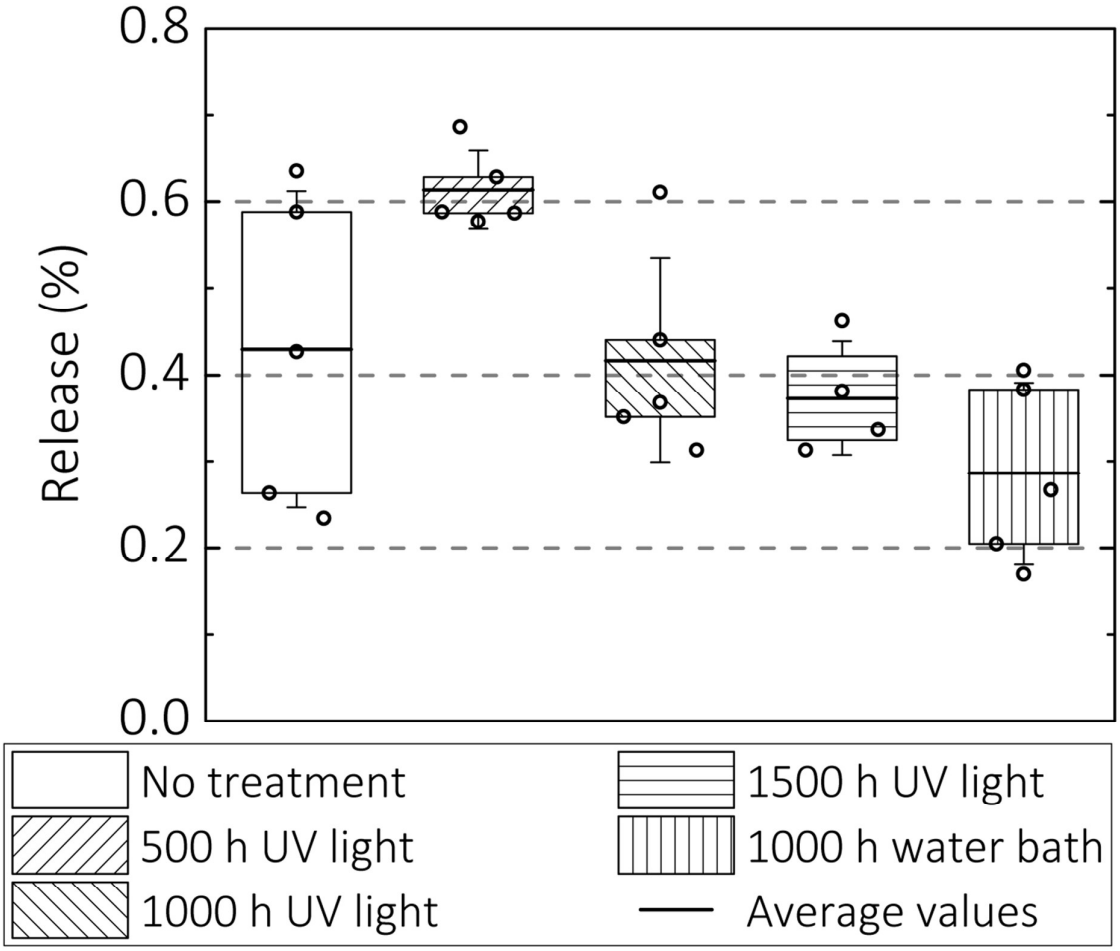


Figure 5: Box plots of the results from the release measurements. Each measurement represents five independent data points, marked by ○. The boxes mark the 25 and 75 % percentiles. Further the average values and the standard deviations are given.

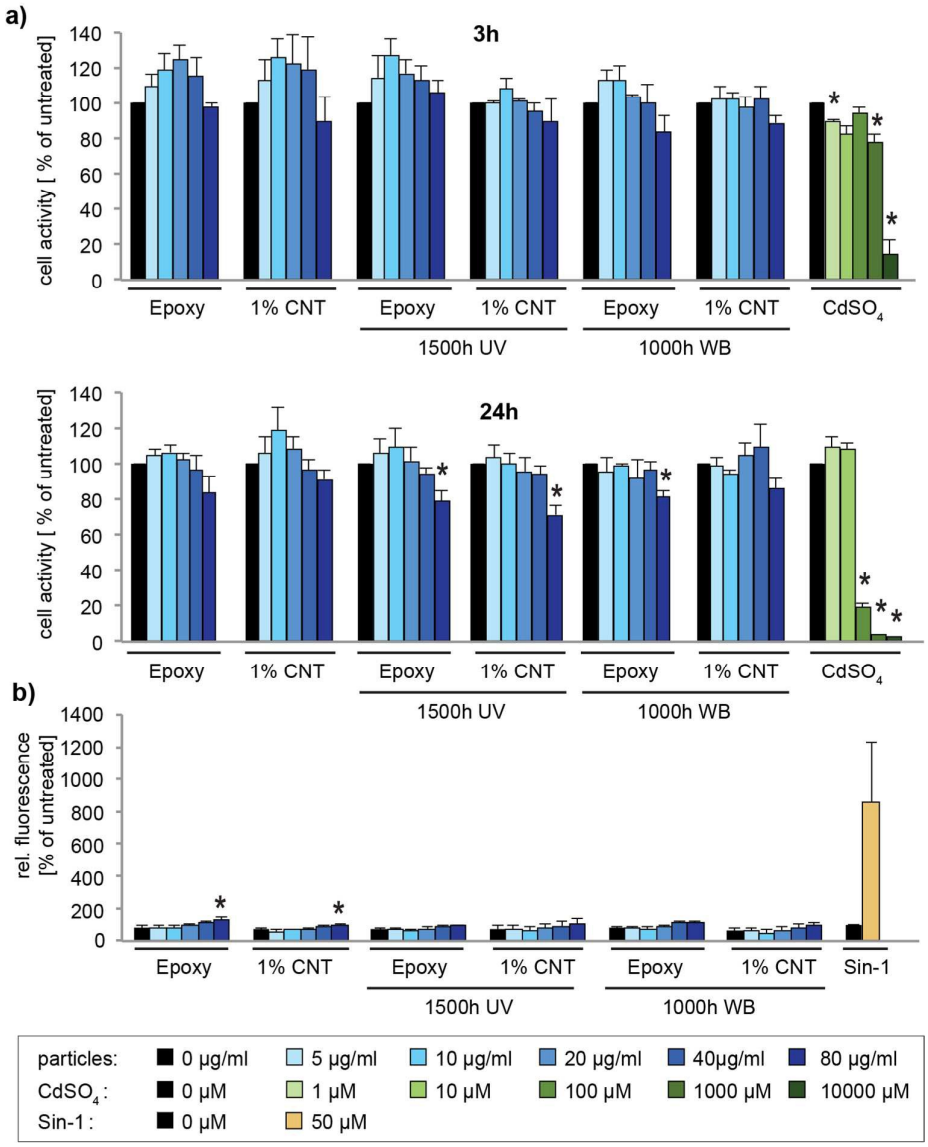


Figure 6: Viability and ROS formation in THP-1 macrophages exposed to abraded particles from control and aged nanocomposite materials. a) PMA-differentiated THP-1 cells were treated with the indicated concentrations of abrasion particles for 3 and 24 h before performing the MTS cell viability assay. $CdSO_4$ was used as the positive control to induce cell death. b) Cells were incubated with abrasion particles and ROS formation was measured after 2 h using the DCF assay. Sin-1, a morpholino compound, was used as a positive control. Data represent the mean ± StEM of three independent experiments.